journal of the mechanical behavior of biomedical materials 163 (2025) 106881

Contents lists available at ScienceDirect

Journal of the Mechanical Behavior of Biomedical Materials

journal homepage: www.elsevier.com/locate/jmbbm

Aortic valve leaflet assessment to inform novel bioinspired materials: Understanding the impact of collagen fibres on the tissue's mechanical behaviour

Celia Hughes [a,b,c], Alix Whelan [a,b,c,d], David O'Reilly [c], Evelyn M. Campbell [c], Caitríona Lally [a,b,d,*]

[a] Trinity Centre for Biomedical Engineering, Trinity Biomedical Sciences Institute, Trinity College Dublin, 2, Dublin, Ireland
[b] Discipline of Mechanical, Manufacturing, and Biomedical Engineering, School of Engineering, Trinity College Dublin, 2, Dublin, Ireland
[c] Structural Heart Division, Boston Scientific Corporation, Galway, Ireland
[d] Advanced Materials and Bioengineering Research Centre (AMBER), Trinity College Dublin, Ireland

ARTICLE INFO

Keywords:
Aortic valve
TAVR
Uniaxial tensile testing
Second harmonic generation
Microstructure

ABSTRACT

Aortic stenosis is a prevalent disease that is treated with either mechanical or bioprosthetic valve replacement devices. However, these implants can experience problems with either functionality in the case of mechanical valves or long-term durability in the case of bioprosthetic valves. To enhance next generation prosthetic valves, such as biomimetic polymeric valves, an improved understanding of the native aortic valve leaflet structure and mechanical response is required to provide much needed benchmarks for future device development. This study aims to provide such information through imaging and mechanical testing of porcine aortic valve leaflet tissue. Using second harmonic generation imaging on cleared tissue it is shown that the fibre orientations are dependent on the leaflet type (left coronary, right coronary, non-coronary), while fibre crimp is not solely dependent on either of these factors. Uniaxial tensile testing of the leaflets and their layers showed that the ventricularis layer is stiffer than the fibrosa but the fibrosa dominates the mechanical response of the whole leaflet due to its higher thickness. Overall, this work provides a detailed assessment of the native porcine aortic valve leaflets' microstructure and mechanical response, delivering key information to aid the design and manufacture of future bioinspired valve implant devices.

1. Introduction

Aortic stenosis is the most prevalent valvular disease requiring surgical or transcatheter intervention in Europe (Iung et al., 2019). Valve replacement options contain both mechanical and bioprosthetic devices which are available and widespread. However, there are still significant challenges to overcome with these devices with regards to their functionality: mechanical heart valves induce thrombosis leading to patients requiring lifelong anticoagulant treatment, and bovine or porcine pericardium used in bioprosthetic heart valves experiences premature deterioration (Otto et al., 2021). An improved understanding of the native valve leaflets' structure and mechanical properties could help inform the next generation of implantable devices and treatments.

By designing new prosthetic valves to mimic the native hemodynamic environment, these devices can achieve the superior function and durability needed from current commercial devices. To be able to develop a truly "bioinspired" material for this application it is essential to have a detailed understanding of the native leaflet material and mechanical response, as well as the underlying microstructure determining this response. Currently, there is a lot of interest in developing this kind of biomimicking device, particularly in replicating the complex collagen fibre structure of the native aortic leaflets (Coulter et al., 2019; Zeugin et al., 2024; Saidy et al., 2019; Stasiak et al., 2020; Boehm et al., 2023; Snyder and Jana, 2023; Vernon et al., 2022). However, across all of these studies it is clear that there is a need for a benchmark, both for the fibrous structure and the mechanical response of the material.

Aortic valve leaflets have been a topic of study for decades, providing a detailed account of the leaflets' function and macrostructure. We know that the leaflets are comprised of the fibrosa, spongiosa, and ventricularis layers which all work together throughout the cardiac cycle.

* Corresponding author. Parsons Building, Trinity College Dublin, College Green, Dublin 2, D02 PN40, Ireland.
E-mail address: lallyca@tcd.ie (C. Lally).

https://doi.org/10.1016/j.jmbbm.2024.106881
Received 11 October 2024; Received in revised form 28 November 2024; Accepted 26 December 2024
Available online 27 December 2024
1751-6161/© 2024 Published by Elsevier Ltd.

The fibrosa layer provides the leaflet with its strength through predominantly circumferentially aligned collagen fibre bundles, while the ventricularis aids opening and closing with radially aligned elastin fibres.

It has been shown that the underlying microstructure of soft biological tissues drives their mechanical properties (Johnston et al., 2021; Lee et al., 2015; Stella and Sacks, 2007; Tornifoglio et al., 2023; Whelan et al., 2019). In leaflet tissue, the mechanical response can vary based on the direction (Stella and Sacks, 2007; Balguid et al., 2007; Billiar and Sacks, 2000; Kalejs et al., 2009; Martin and Sun, 2012; Mavrilas and Missirlis, 1991; Rassoli et al., 2024; Stradins et al., 2004; Vesely, 1997; Vesely and Noseworthy, 1992) and the layer (Stella and Sacks, 2007; Vesely, 1997; Vesely and Noseworthy, 1992) tested. In particular, the fibre orientation and degree of collagen straightness or crimp is known to determine the stiffness and strain-stiffening behaviour in pericardial tissue used in leaflets of bioprosthetic valves (Whelan et al., 2021). Histology has commonly been used to visualise the leaflet microstructure; however, it is time consuming, destructive, and only able to provide a discrete profile of tissue structure in one plane (Lee et al., 2015; Martin and Sun, 2012; Gross and Kugel, 1931; Hepfer et al., 2018; Joyce et al., 2009; Pierlot et al., 2015; Sacks et al., 1998). Sacks et al. used small angle light scattering (SALS), a non-destructive transmissive light-based technique, to identify dominant fibre orientations and dispersion on glycerol-cleared aortic valve tissue to measure changes in fibre orientation with increasing fixation pressures (Sacks et al., 1998). SALS has since been used on valve leaflet tissue to measure microstructural changes (Joyce et al., 2009; Liao et al., 2008; Manji et al., 2015). However, it is only able to identify a singular, average fibre orientation throughout a sample depth which reduces its ability to identify the presence and orientation of more than one family of fibres. Additionally, to obtain information from a singular layer, the leaflet needs to be separated. This separation results in stretching of the fibrosa and contraction of the ventricularis which can give an inaccurate depiction of the fibre orientations in a whole, intact leaflet *in vivo* (Stella and Sacks, 2007). Mega et al. and Rock et al. used white and polarised light microscopy to obtain images of the aortic leaflets and identify large-scale fibre bundles across the surface of the fibrosa, respectively (Mega et al., 2016; Rock et al., 2014). While these have been able to show the presence of multiple fibre families, they lack the detail of localised fibre orientation and dispersion, and only represent the fibrosa layer. Ultimately, these studies have been unable to provide detailed information of the collagen microstructure of both the fibrosa and ventricularis layers in whole, intact leaflets.

Second harmonic generation (SHG) microscopy is a non-destructive, two-photon imaging technique commonly used to obtain high resolution images of collagen microstructure throughout various thickness in tissues (Chen et al., 2012; Campagnola and Dong, 2011). It has been used to qualitatively assess microstructure changes in pulmonary leaflet tissue (Hepfer et al., 2018; Manji et al., 2015), to quantify collagen characteristics in aortic leaflet belly (Hutson et al., 2016), and quantify fibre orientation and dispersion in mitral leaflets (Sadeghinia et al., 2022). However, a key limitation of SHG is its inability to penetrate tissue depths greater than 150 μm (Whelan et al., 2021; Campion et al., 2021; Torun et al., 2023). To improve this, Schriefl et al. and Sadeghinia et al. used a benzyl alcohol and benzyl benzoate (BABB) solution on arterial tissue and mitral leaflets, respectively, to clear the tissue and achieve images at depths greater than 1 mm (Sadeghinia et al., 2022; Schriefl et al., 2013). BABB is a hydrophobic tissue clearing method that causes delipidation to minimise light scattering within the tissue without altering collagen structure; consequently, it results in minor tissue shrinkage (Ueda et al., 2020).

While aortic valve leaflets have frequently been a topic of study, there is a lack of detailed information on the collagen microstructure. Particularly, there is a gap in discerning the difference in structure between the fibrosa and ventricularis leaflet layers in intact leaflets. To better understand the microstructure, we aim to draw inspiration from previous studies and use SHG to assist with quantifying fibre orientation and crimp in the commissure and belly regions of BABB-cleared porcine aortic valve leaflets.

Additionally, mechanical testing has been performed on aortic valve leaflets from both humans and animals, employing uniaxial (Balguid et al., 2007; Kalejs et al., 2009; Mavrilas and Missirlis, 1991; Rassoli et al., 2024; Stradins et al., 2004; Vesely, 1997; Vesely and Noseworthy, 1992) and biaxial (Stella and Sacks, 2007; Billiar and Sacks, 2000; Martin and Sun, 2012; Rassoli et al., 2024) methods. While there is a similar range in results through all of these studies, each uses different testing protocols and data processing methods, leading to inconsistent results that cannot be reliably compared or combined. Biaxial testing has provided valuable insight into leaflet mechanics, but by design it prevents studying the response of tissues in particular orientations decoupled from other directions, information which is useful for developing new materials. Additionally, only two studies separate the leaflets into layers (Stella and Sacks, 2007; Vesely and Noseworthy, 1992); however, neither of these studies considered tissue thickness, opting only to measure tension rather than stress. It is important to consider both the material and the mechanical response of these leaflet layers when exploring material alternatives. In the screening of new materials, medical device companies and researchers often use quick and effective methods, such as uniaxial tensile testing, to characterise a decoupled mechanical response, and they need a reliable baseline to compare to. However, the current literature does not deliver on this need.

To supplement the structural information gained from imaging, the aim of this study is to perform uniaxial tensile testing on strips from whole porcine aortic valve leaflets as well as their fibrosa and ventricularis layers. By combining both imaging and mechanical testing on this tissue, we can develop a detailed profile of the mechanical behaviour of the leaflets and their individual layers and, importantly, understand how the underlying collagen microstructure governs this behaviour to ultimately provide key information for the development of novel, bioinspired materials for future prosthetic valves.

2. Methods

2.1. Tissue dissection and freezing

Sixteen porcine hearts from 6-month-old Large White Pigs were acquired from a local abattoir (N = 10 for mechanical testing, N = 3 for histology, and N = 3 for SHG), with n = 3 aortic valve leaflets available from each heart. Within three hours of slaughter, each leaflet was carefully dissected from the aortic root. After rinsing in phosphate buffered saline (PBS) (P5493, Sigma), each leaflet was cryopreserved in a tissue freezing medium containing Gibco RPMI medium (21875034, BioSciences), sucrose (S0389, Sigma), and dimethylsufoxide (PIER20688, VWR International) to −80 °C at a controlled rate of 1 °C/min in a Mr. Frosty container (Nalgene, USA). Using dimethylsufoxide as a cryoprotectant prevents the formation of ice crystals during freezing that could possibly damage the tissue microstructure (Müller-Schweinitzer, 2009). Rapid thawing of each sample occurred at room temperature within two months of freezing and each sample was rinsed in PBS immediately after thawing to remove excess solution.

2.2. Histology

To conduct histological analysis, porcine leaflets from N = 3 animals (n = 3 leaflets each) were cut into 2–3 mm sections along either the radial or circumferential direction and fixed in 0.6% glutaraldehyde solution overnight. Samples were stepwise dehydrated (Leica TP1020, semi-enclosed benchtop tissue processor, Germany), embedded in paraffin wax blocks, and sectioned in 8 μm-thick slices using Feather C35 microtome blades. This yielded cross sections in the radial and circumferential direction through the leaflet's thickness. Sections in each direction were stained using Verhoeff's elastin (VF) for elastin and

both Picrosirius red (PSR) and Alcian blue (AB) for the combination of collagen and glycosaminoglycans (GAG) (Leica ST5010, Autostainer XL, Germany). Brightfield images were obtained using an Aperio CS2 microscope with ImageScope software V12.3 (Leica Biosystems Imaging, Inc., Vista, California).

2.3. Second harmonic generation (SHG) imaging

2.3.1. Clearing protocol

Leaflets from N = 3 animals were used for imaging to allow for n = 3 left coronary (LC), n = 3 right coronary (RC), and n = 3 non-coronary (NC) leaflets, resulting in n = 9 total leaflets imaged. After defrosting, the leaflets were fixed in 0.6% glutaraldehyde solution overnight; each sample was placed in a histology cassette and held securely between sponge sheets to ensure a flat surface for imaging and minimise shrinkage in the circumferential and radial directions. Tissues samples were chemically cleared according to a protocol described previously (Sadeghinia et al., 2022; Schriefl et al., 2013) using a 1:2 BABB solution. Briefly, samples were dehydrated in a series of graded alcohol solutions (50%, 75%, 95%, 95%, 100%, 100%) for 45 minutes at a time then submerged in a 1:1 solution of alcohol to BABB for 4 hours, before finally submerging in 100% BABB overnight (~18 hours). Samples were imaged within 2 days of clearing.

2.3.2. Imaging

SHG imaging was carried out using a Carl Zeiss 710 NLO Microscope (Carl Zeiss, Jena, Germany) and a laser wavelength of 840 nm. Z-stacks and tiled scans (5x5 tiles for belly region, 3×8 tiles for commissures) were taken at a magnification of 20× through the maximum thickness available, with a tile depth between 20 and 25 μm, depending on sample thickness. Each leaflet was imaged at both the belly region and a commissure, see Fig. 1A.

2.3.3. Image processing

For image processing, tiles from each scan were selected for analysis. As the leaflets thickness is nonuniform, the number of images containing tissue differed by region. Therefore, for each stack, the topmost image with visible tissue was selected for analysis followed by each subsequent 3rd image until the tissue was no longer visible, see Fig. 1B. This resulted in an analysed image every 60–75 μm over regions ranging from 200 to 900 μm in total thickness.

Image processing was carried out with FIJI software (Schindelin et al., 2012) using the NeuronJ plugin (Meijering et al., 2004) to measure fibre crimp as described by Rezakhaniha et al. (2012) and Whelan, 2021 (Rezakhaniha et al., 2012; Whelan, 2021). Crimp was measured by degree of fibre straightness (S), defined based on the length of the fibre (L_c) and the straight distance between the endpoints (L_0):

$$S = \frac{L_0}{L_c}$$

where S is bound between 0 and 1, with 1 representing a completely straight fibre. Straightness measurements (n = 3) were taken per image, resulting in ~50 measurements per belly or commissure, see Fig. 1B. In addition, measurements of the dominant fibre orientations (n = 3) were taken for each image of the fibrosa. In total ~900 measurements of straightness and ~550 measurements of fibre angle were taken for analysis.

2.4. Uniaxial tensile testing

2.4.1. Tissue preparation

Uniaxial tensile testing was performed on test strips. Strips were prepared in either the circumferential (C) or radial (R) directions from whole leaflets (n = 7C/10R), fibrosa layers (n = 12C/11R), or ventricularis layers (n = 8C/8R), see Fig. 1C. To obtain fibrosa and ventricularis layers, the layers were separated by pinning the leaflet fibrosa side down onto a cardboard mat at 4–6 points, depending on the size of the sample, along the outer edge. Using forceps and a scalpel, the ventricularis was carefully removed from the fibrosa by scoring the spongiosa, starting from the belly edge of the leaflet until reaching the free edge, similar to previously described methods (Stella and Sacks, 2007; Vesely and Noseworthy, 1992).

Before testing, the samples were separated into 3–4 mm wide rectangular strips in either the circumferential or radial direction using a scalpel, see Fig. 1C. After cutting, the tissue was free to stretch or contract in width, giving a resulting width for each sample between 1 and 3 mm. For each strip, thickness measurements were taken at three locations along the gauge length using a Mitutoyo LITEMATIC VL-50 thickness gauge (Mitutoyo (UK) Ltd., UK). This machine has an accuracy of 0.5 + h/1000 μm, where h is the height of the sample being measured.

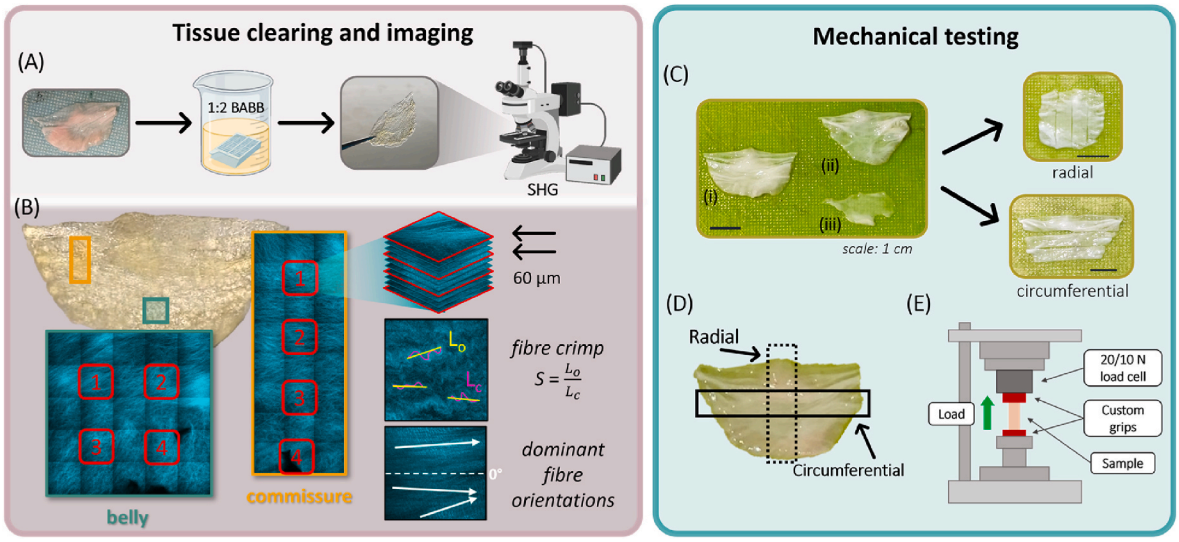

Fig. 1. Overview of methods used in this study. (A) Clearing porcine valve leaflets using 1:2 BABB and SHG imaging, (B) acquisition and analysis. (C) Separation of (i) whole leaflets into (ii) fibrosa and (iii) ventricularis layers, and further into strips in the radial and circumferential directions. (D) Diagram of radial and circumferential directions on intact leaflet and (E) diagram of uniaxial tensile testing setup.

2.4.2. Mechanical testing

To prepare for testing, samples were loaded into custom-made grips and a holder used for preparation. Samples were held within grips lined with Velcro and secured at the very ends with a drop of superglue, with care taken to ensure glue did not get on the sample gauge length. Once in the grips, the samples were held taught within the holder and the width was measured at three points along the gauge length using an Absolute AOD Digimatic calliper (Mitutoyo (UK) Ltd., UK).

Each sample was uniaxially extended to failure using a Zwick uniaxial testing machine (Zwick Roell Group, Ulm, Germany) with either a 20 N (whole samples, fibrosa circumferential) or a 10 N load cell (ventricularis, fibrosa radial). With a strain rate of 20 mm/min, each sample was preconditioned for 5 cycles from 0.05 to 0.1 MPa and then loaded in tension until failure (defined as a 20% drop from maximum load reached), in line with previous testing performed within the group (Whelan et al., 2019). Sample displacement and load was measured using the Zwick crosshead output and a new reference configuration was recorded after preconditioning. Every sample was hydrated with PBS and tested at room temperature.

2.4.3. Mechanical characterisaion

Each sample was characterised by its initial and final modulus, calculated from the slope of both the true stress and tension curves. True stress was defined as:

$$\sigma_t = \sigma_{eng}\left(1 + \varepsilon_{eng}\right)$$

Where σ_{eng} is engineering stress and ε_{eng} is engineering strain, defined as:

$$\varepsilon_{eng} = \frac{\Delta l}{l_0}$$

Where Δl is crosshead displacement and l_0 is initial sample gauge length. True strain was defined as:

$$\varepsilon_t = ln\left(1 + \varepsilon_{eng}\right)$$

Tension was defined as:

$$Tension = \frac{force}{sample\ width}$$

Modulus values were calculated using the slope formula:

$$m = \frac{y_2 - y_1}{x_2 - x_1}$$

With initial moduli taken as the slope for the initial part of the curve, which was defined as the region before a 5% increase from the starting slope as this was the point when the samples typically began to stiffen. Final moduli were taken as the slope between failure and 80% of the failure load to obtain a robust determination of the slope at the end of the curve.

2.4.4. Data processing

All processing from raw, Zwick-output data was carried out using a custom MATLAB script to return true stress/strain, tension/strain, and slope values.

2.5. Statistics

All statistical analysis was performed using GraphPad Prism 9 (GraphPad Software, Inc., San Diego, California). Specific statistical tests for each dataset and sample sizes are specified in the results section. All numerical and graphical values are shown as mean ± standard deviation, and a $p \leq 0.05$ was considered significant.

3. Results

3.1. Histology

Histological images of leaflet samples sliced either along the circumferential or radial direction were obtained, see Fig. 2. Combining PSR and AB allows the three layers of the leaflets to be distinguished, i.e. the fibrosa is on the top densely packed with collagen, the ventricularis on the bottom, with the spongiosa, rich in GAGs (blue), separating them. The coherent orientation of collagen fibres in the circumferential direction can be seen in the fibrosa, while there is no clear preference of collagen fibre orientation in the ventricularis layer, see Fig. 2A and B. Looking at the VF-stained samples, the elastin in the leaflets is primarily located in the ventricularis, in what look like sheets somewhat more preferentially aligned along the radial direction of the leaflet, see Fig. 2C and D.

3.2. SHG imaging

3.2.1. Qualitative analysis

Fig. 3 shows the images of the collagen fibre structure throughout the leaflet thickness at the belly and commissure regions across the three leaflet types; the number of image tiles differed based on the total sample thickness. In all leaflets, the collagen microstructure in the fibrosa appears dense and organised around one or two primary directions, see Fig. 3. Moving through the leaflet thickness this structure becomes sparser and more dispersed in the ventricularis, with random alignment of collagen fibres.

3.2.2. Fibre straightness

Across all the leaflets studied, collagen fibres are more crimped in the fibrosa than the ventricularis, see Fig. 4B. Overall, for all of the leaflets together, the level of fibre straightness remains consistent within each layer across the regions studied (fibrosa belly/commissure: 0.68 ± 0.12/0.68 ± 0.13; ventricularis belly/commissure: 0.79 ± 0.10/0.78 ± 0.10).

When grouping the results based on animal (PAV 1, 2, and 3) or leaflet type (LC, RC, NC), there is no trend to suggest that fibres are more or less straight based on either of these factors, and the fibrosa remains more crimped than the ventricularis, see Fig. 4C–F. For detailed straightness measurements, see supplementary material.

These results are presented to appreciate the overall distribution of fibre crimp across all leaflets and animals. While the number of observations are high (n = 54–273), this represents a small population of animals (N = 3). To avoid pseudoreplication inflating statistical significance, the results presented here do not include statistical analysis (Lazic, 2010). For this analysis, see supplementary material.

3.2.3. Fibre orientation

Dominant collagen fibre orientations were measured in the fibrosa layer of the leaflets, shown in Fig. 5A–D. The ventricularis was not considered in the orientation analysis due to the high degree of disorganisation of the fibres in this layer resulting in no clear dominant alignment. There is a larger spread of angles in the belly portion of the leaflet compared to the commissure region, with the suggestion of a bimodal distribution at the belly region, see Fig. 5A and B. For the belly, the angles are centred around −10 and + 15° while in the commissure the angles are normally distributed around −11°.

Looking at differences in fibre orientation between valves and leaflet type in both the belly (B) and commissure (C) regions, the mean fibre orientations differ more between leaflet types than between animals, suggesting that fibre orientation is dependent upon leaflet type rather than animal, see Fig. 5C and D.

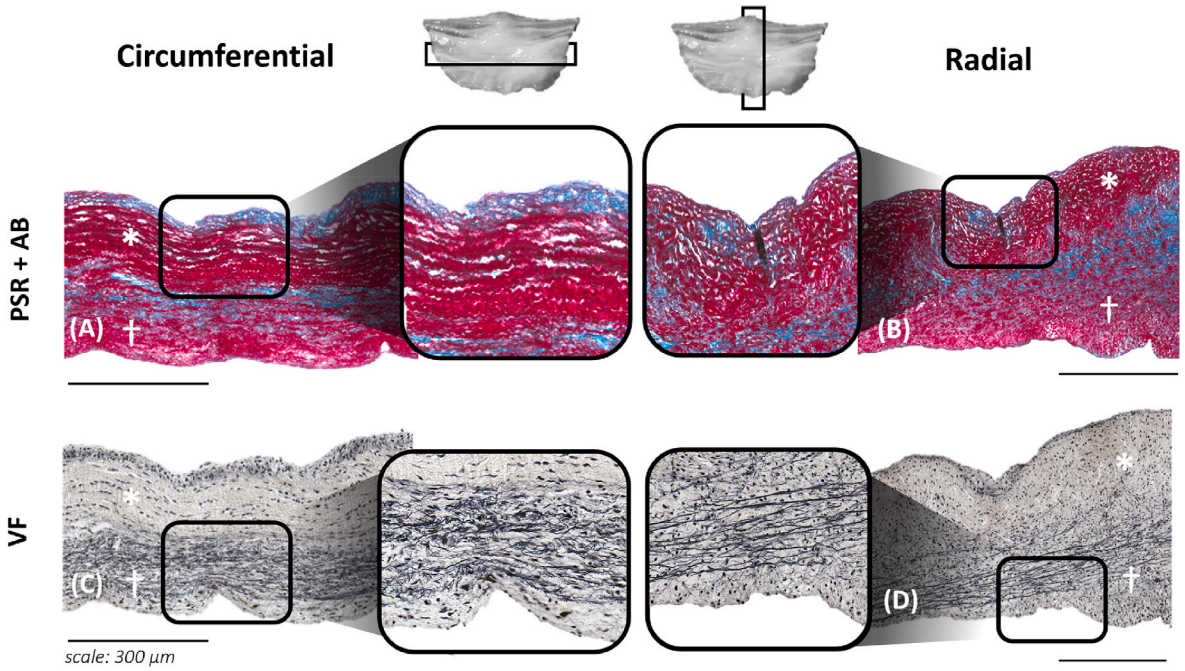

Fig. 2. Representative histology images of sample slices in the circumferential and radial directions stained with PSR and AB for collagen (red) and GAG (blue) (A, B), and the slices from the same samples stained with Verhoeff's for elastin (black) (C, D). Samples are oriented with the fibrosa layer (*) at the top and ventricularis (†) at the bottom. (For interpretation of the references to colour in this figure legend, the reader is referred to the Web version of this article.)

3.3. Uniaxial tensile testing

3.3.1. Leaflet and layer thickness

The fibrosa samples were significantly thicker than the ventricularis samples (0.33 ± 0.13, $n = 23$ and 0.06 ± 0.03 mm, $n = 15$, respectively; $p = 0.0002$), and both groups were significantly thinner than the whole, intact samples (0.53 ± 0.15 mm, $n = 17$; $p = 0.0165$ for fibrosa and $p < 0.0001$ for ventricularis), see Fig. 6A.

3.3.2. Stress and tension response

For each group, an increase in mean modulus was observed between the initial and final portions of the curve, see Fig. 6B–D. Generally, the circumferential samples had a stiffer response than the radial samples, although only the fibrosa exhibited a statistically significant difference between the two orientations in both the initial (5.70 ± 0.09, $n = 5$ and 1.28 ± 1.69 MPa, $n = 7$ for circumferential and radial, respectively) and final (26.6 ± 12.09, $n = 6$ and 2.07 ± 0.92 MPa, $n = 7$ for circumferential and radial, respectively) portions of the curve. Across the board, there were no statistically significant differences between the fibrosa, ventricularis, and whole leaflet samples tested in the circumferential direction, in either portion of the curve. This also remained the case for the radial direction. Unexpectedly, for samples tested in the circumferential direction, no significant difference was found between the ventricularis and either the fibrosa or whole leaflet, with the mean modulus values remaining above the others for both the initial (28.44 ± 36.6 MPa, $n = 6$) and final (42.48 ± 14.81 MPa, $n = 6$) modulus values. This relationship was also seen in the radial direction for the final modulus (54.14 ± 30.75 MPa, $n = 6$). It is worth noting, however, that in in both radial and circumferential groups there is a high amount of variability in the ventricularis response.

In addition to stress, tension was analysed to investigate the influence of sample thickness on the load bearing share of the tissue, see Fig. 6E–G. By removing thickness from the calculation, tension gives a better representation than stress response for how the individual layers contribute to the overall leaflet load bearing. Here, we see greater differences between the groups tested. The fibrosa and whole leaflet groups exhibit significantly stiffer behaviour in their circumferential directions compared to radial in both the initial ($p = 0.0001$ for FC and FR; $p = 0.014$ for WC and WR) and final ($p < 0.0001$ for RC and FR; $p = 0.0015$ for WC and WR) regions. There was no statistical difference observed between the two ventricularis directions for either portion of the curve. Between the groups, for samples tested in the circumferential direction, the ventricularis was significantly less stiff than the fibrosa ($p = 0.0093$) and whole leaflet ($p = 0.0012$) in the initial region and remained significantly less stiff than the whole leaflet ($p = 0.0243$) samples in the final region. Across all the groups and both regions, there were no statistically significant differences between any of the radial samples.

Due to a number of samples breaking at the grips, failure stress and strain are not reported, instead only initial and final moduli have been considered.

4. Discussion

This study presented the use of histological imaging, SHG imaging, and uniaxial tensile testing to characterise the mechanical response and collagen microstructure of healthy, porcine aortic valve leaflets and their fibrosa and ventricularis layers with the aim of providing benchmarks for development of novel synthetic devices. This work presents, for the first time, the use of the chemical clearing agent BABB on aortic valve leaflets to allow for SHG imaging and detailed analysis of the collagen microstructure throughout the entire leaflet thickness, something which has previously been a challenge for imaging of valve leaflet tissue.

To effectively replicate native aortic leaflet tissue with synthetic materials, the collagen microstructure should be considered as the fibre orientation and organisation determine the tissue's function. Using SHG paired with BABB gave valuable insights into the collagen microstructure at key locations in the leaflets. Chemically clearing the leaflets with BABB solution allowed for full penetration of the leaflet thickness, up to 900 μm at some locations, while without clearing SHG depth is usually limited to less than 150 μm (Whelan et al., 2021; Campion et al., 2021; Torun et al., 2023). This resulted in the ability to obtain detailed images of the collagen microstructure throughout the whole tissue thickness without the need for destructive wax embedding and slicing that comes

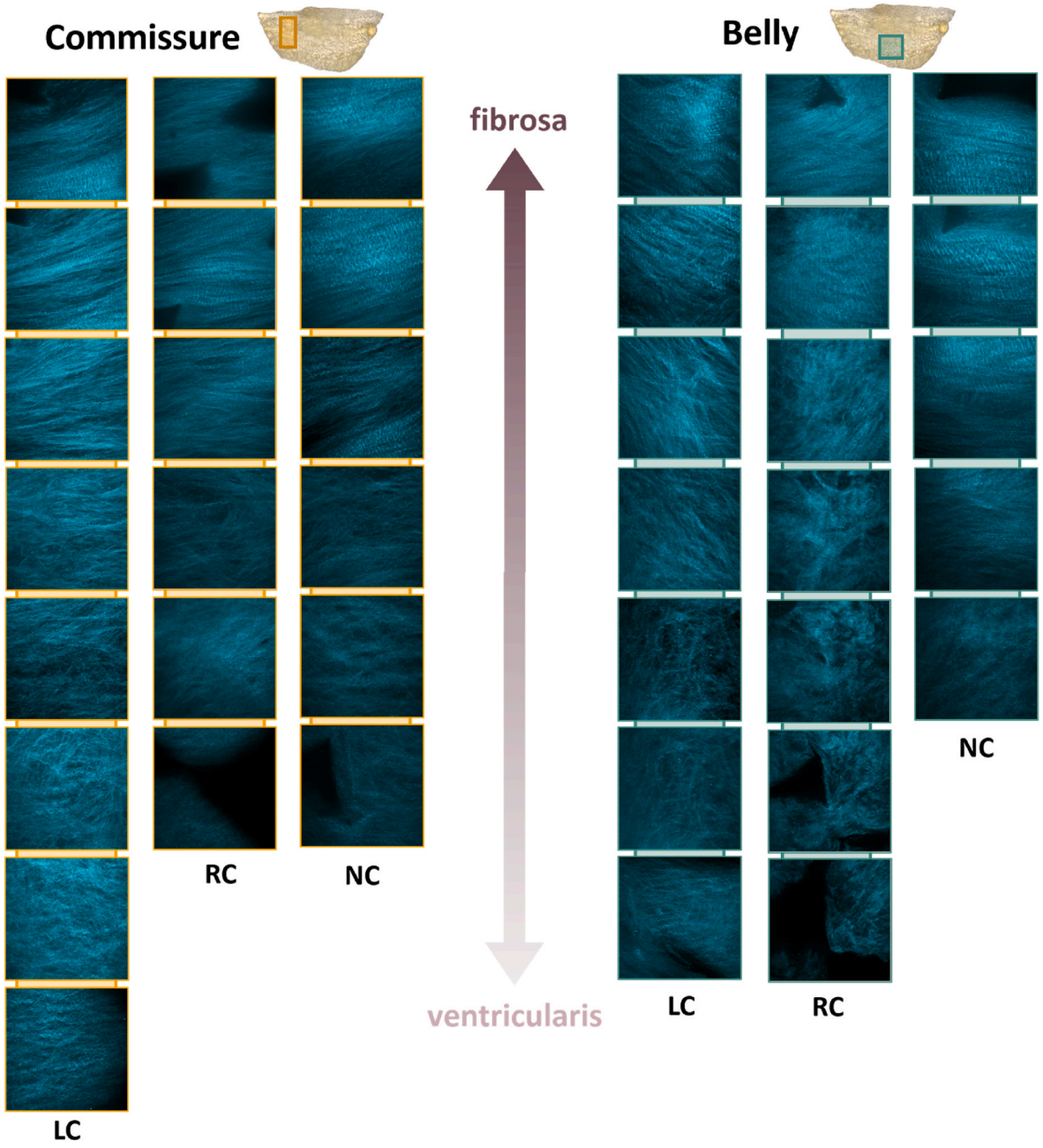

Fig. 3. Representative SHG images from each leaflet type (left coronary, LC; right coronary, RC; and non-coronary, NC) at both the commissure and belly regions. Each column shows a single tile view of the collagen microstructure from the fibrosa layer down through the thickness to the ventricularis. Distance between individual tiles: 60–75 μm. Tile size: 425 × 425 μm. More sample images in supplementary.

with histology.

While this study investigates fibre orientation and crimp, the images obtained can be used to extract other useful characteristics of the microstructure. For example, Whelan et al. used SHG images to quantify collagen content in bovine pericardium (Whelan et al., 2021) which could be applied to this workflow to extract potentially further differences between the fibrosa and ventricularis layers. Another application is in the development of more refined constitutive models to describe this tissue, such as in Sadeghinia et al. who utilised SHG on cleared mitral valve tissue (Sadeghinia et al., 2022). Ultimately, SHG imaging on cleared leaflet tissue can provide numerous insights into the tissue microstructure in a more robust and time efficient process than histology.

Collagen crimp is a key feature of tissue microstructure as it governs the tissue's strain-stiffening behaviour. With the aortic valve, the degree of crimp determines how much the leaflets are able to stretch under pressure when closed. To the authors' knowledge, these results have presented the most extensive quantification of collagen crimp to date in the fibrosa and ventricularis layers of the leaflet. We show that when the leaflet is flat, the collagen fibres in the ventricularis are straighter than in the fibrosa layers, see Fig. 4B. Previously, Sacks et al. (1998) used SALS to suggest that the fibres in the ventricularis layer are more crimped than the fibrosa due to lower fibre eccentricity measured compared to the fibrosa. With the new insights from our results, we can see that this particular phenomenon measured by Sacks et al. may not be due to less straight fibres, but most likely from to the higher degree of disorganisation of collagen fibres in this layer. These findings support the known function of the aortic valve: the ventricularis is held in

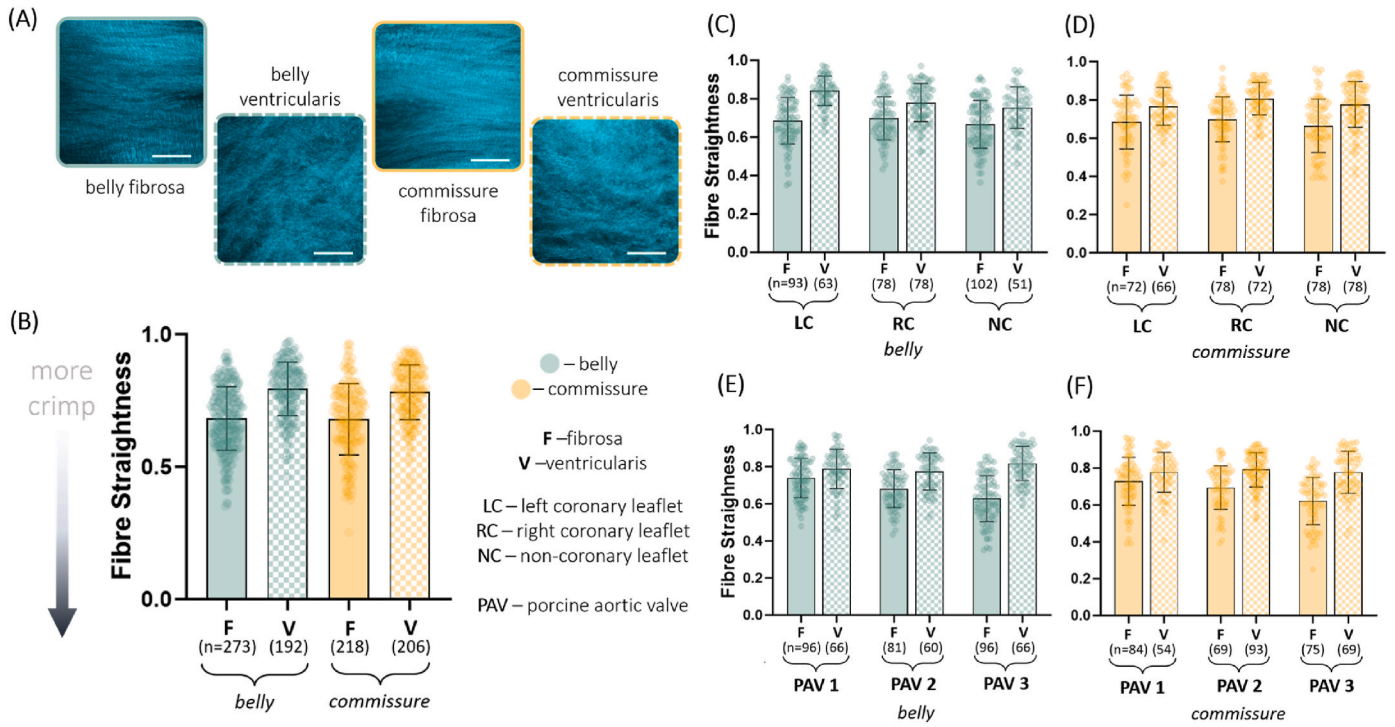

Fig. 4. Overview of fibre crimp analysis measured using fibre straightness, with (A) representative SHG images for each location and layer. (B) All straightness measurements organised by layer and location, (C) for the belly region separated by layer and leaflet type, (D) for commissure region separated by layer and leaflet type, (E) for belly regions separated by layer and animal, (F) for commissure region separated by layers and animal. Scale: 100 μm; n refers to number of measurements from N = 3 valves.

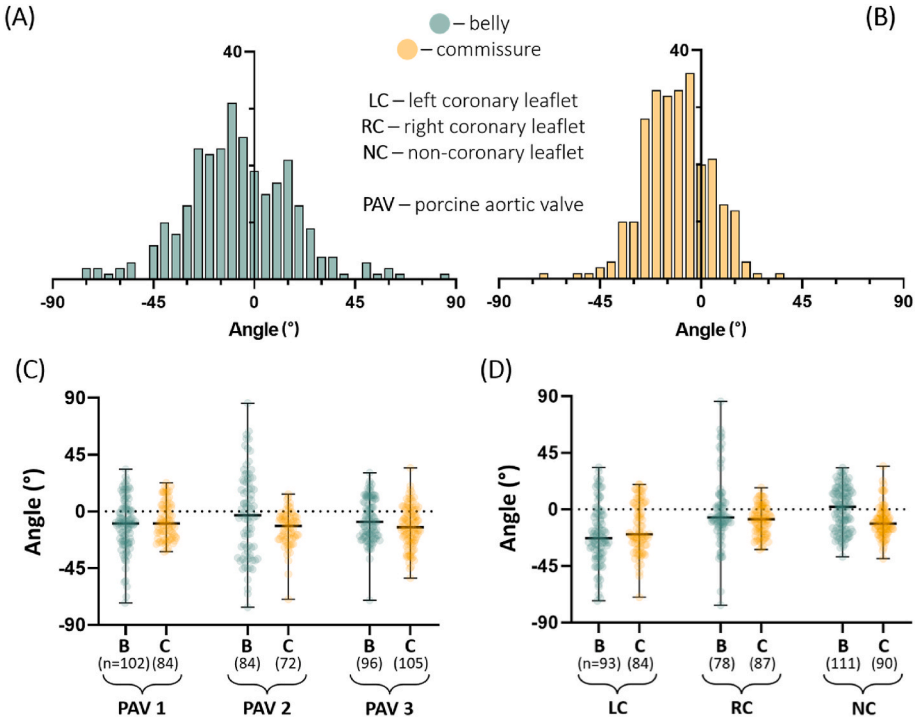

Fig. 5. Fibre orientation analysis in fibrosa layer. Histograms of fibre orientations in (A) belly and (B) commissure regions, for both plots bin width: 5°. Fibre orientations separated by (C) leaflet region and valve, (D) leaflet region and type. n refers to number of measurements from N = 3 valves.

tension to be able to provide elastic recoil to open the leaflet, while the fibrosa contains significant folding to allow leaflet deformation and effective closure of the valve. Throughout leaflet separation during mechanical testing this contrast between the two layers was evident with notable contraction of the ventricularis, particularly in the radial direction, and expansion of the fibrosa after separation (this can be seen in Fig. 1C). This observation is supported by Stella and Sacks (2007) who previously quantified the contraction of the ventricularis and expansion

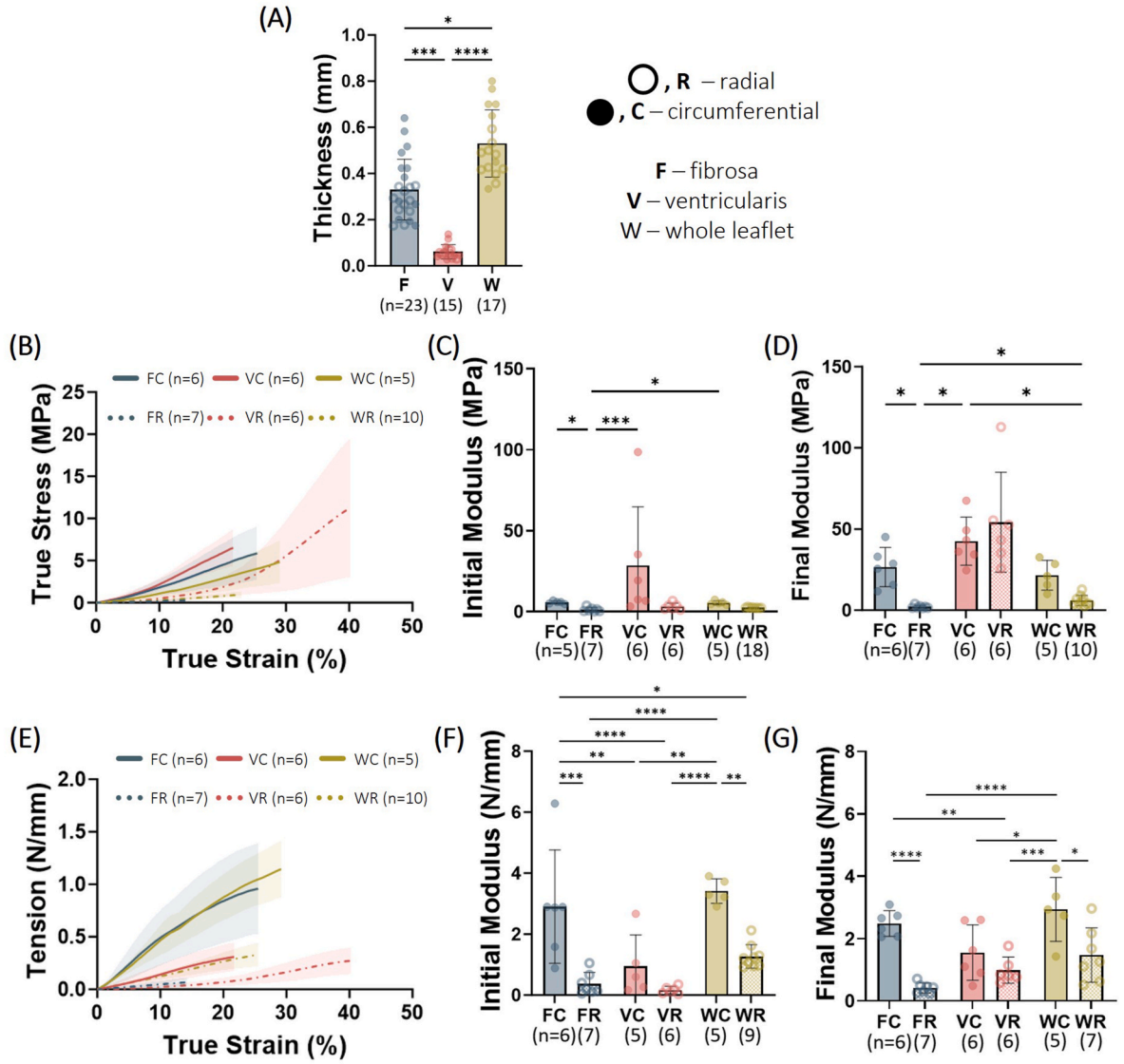

Fig. 6. Uniaxial tensile testing data overview. (A) Thickness measurements for all samples, significance tested using Kruskal-Wallis with Dunn's multiple comparisons test. (B) Average true stress and strain curves for all samples. (C) Initial stress modulus values, significance tested using Kruskal-Wallis with Dunn's multiple comparisons test; 3 outliers removed using ROUT (Q = 1%). (D) Final stress modulus values, significance tested using Brown-Forsythe and Welch ANOVA tests with Dunnett's multiple comparisons. (E) Average tension and true strain curves for all samples. (F) Initial tension modulus values, significance tested using ordinary one-way ANOVA with Tukey's multiple comparisons; 2 outliers removed using ROUT (Q = 1%). (G) Final tension modulus values, significance tested using ordinary one-way ANOVA with Tukey's multiple comparisons test. Normality tested for in all data using Shapiro-Wilk test; $p^{*} \leq 0.05$, $P^{**} \leq 0.01$, $p^{***} \leq 0.001$, $p^{****} \leq 0.0001$. (For interpretation of the references to colour in this figure legend, the reader is referred to the Web version of this article.)

of the fibrosa after separation from each other.

Collagen fibre orientation in the fibrosa layer was quantified in both the commissure and belly regions and supported trends previously noted: there is a higher degree of alignment at the leaflet commissure with the origin of fibre bundles which fan out to a more dispersed overall alignment in the belly region (Sacks et al., 1998; Rock et al., 2014; Misfeld and Sievers, 2007). Previously, studies have only been able to identify either overall fibre orientation in a particular region of interest which removed the ability to identify multiple families of fibres or have only visualised the large-scale fibre bundles across the leaflet (Mega et al., 2016; Rock et al., 2014). While previous work has been useful to understand the overall collagen fibre directions in the leaflet as a whole, a more detailed understanding of the range and variability of fibre orientations was needed and has now been uncovered from the results presented here. These results have been able to show orientation changes in the collagen fibres throughout the layers of the leaflet, something that has not been seen in detail with previously used imaging techniques (Martin and Sun, 2012; Hepfer et al., 2018; Pierlot et al., 2015; Sacks et al., 1998; Liao et al., 2008; Mega et al., 2016; Rock et al., 2014). While fibre orientation was not measured in the ventricularis due to the high degree of disorganisation of the fibres, qualitative assessment of the images shows a stark contrast between the highly organised and dense collagen network in the fibrosa and a more sparse, non-uniform network in the ventricularis (see Fig. 3).

Notably, these results have shown how fibre crimp and orientation change based on leaflet type and between valves. Collagen crimp was not seen to change from animal to animal, suggesting this feature is dependent upon the localised physiological environment of the individual leaflet. Meanwhile, fibre orientation was seen to depend on leaflet type, something that has only previously been seen on a macro scale (Mega et al., 2016; Rock et al., 2014). These results corroborate, at a microscale, what has been seen at a larger scale: predominant fibre orientation in the commissure points downwards towards the centre of the leaflet and belly region, and there is a greater range of fibre

orientations in the belly spanning directions pointing upwards towards both commissures.

The native aortic valve leaflet is a complex structure whose function and mechanical response is dictated by its fibrosa and ventricularis layers. To understand and replicate the native leaflet through novel materials it is essential to characterise not only the leaflet as a whole but also its layers. Uniaxial tensile testing provided these unique insights into the mechanical and material response of the native aortic valve leaflets and their individual layers. In utilising uniaxial over biaxial tensile testing we were able to decouple the circumferential from radial fibre orientations, allowing for the characterisation of the material with fibres predominately orientated either with or against the load. While biaxial testing provides insight into the behaviour of the leaflets *in vivo*, this does not necessarily directly translate to screenable characteristics in new materials for prosthetic leaflets. When screening new materials, medical device companies or researchers will use quick and reliable procedures like uniaxial testing to determine the mechanical response and anisotropy of the material, and they need to have accurate baseline data for assessment. To compare the groups, we looked at the stress and tension versus strain response curves as well as the initial and final modulus values for each of these. While all of the samples were loaded until failure, it was noted that many samples failed at the grips, suggesting high stress concentrations at these locations; for this reason, failure stress and strain have not been reported or considered in analysis. This is expected when strip samples are used over dog-bone samples (Pei et al., 2021).

In the whole, intact leaflets we saw that the tissue was stiffer in the circumferential direction than the radial direction, with a higher tensile modulus in both the initial and final loading regions. A handful of studies have previously investigated the uniaxial tensile response of this tissue before, looking at both porcine and human aortic valve tissue, and the results obtained in this current study fall within a similar range, see Fig. 3 in supplementary material (Balguid et al., 2007; Kalejs et al., 2009; Mavrilas and Missirlis, 1991; Stradins et al., 2004). Each of these studies employed a different testing protocol with varying stain rates and preloading conditions, so in order to reliably compare whole leaflet uniaxial behaviour to the individual layers it was necessary to repeat these tests.

By not only analysing the stress response of the tissue but also the tension response we used the initial and final moduli to show how the thickness of the layers impacts their mechanical contribution in the whole leaflet. Most notably, we see that the ventricularis as a material is very stiff, with many samples reaching higher stresses in both the radial and circumferential directions than the fibrosa. This high stiffness in both directions can be attributed to the disorganised nature of the collagen fibres, evident through histology and SHG imaging, allowing for a stiff response in all directions. Due to the tissue's small thickness, however, it does not dominate the leaflet's stress response in the circumferential direction. This is clearly shown in Fig. 6B and E as the whole leaflet's stress and tension response more closely follow that of the fibrosa rather than the ventricularis in the circumferential direction. Due to its larger thickness and more specialised collagen fibres alignment, the fibrosa is the primary contributor to the leaflet's ability to withstand stress circumferentially.

Meanwhile, in the radial direction, it is the essential combination of both the ventricularis and fibrosa that provide the leaflet's mechanical response. These results further support conclusions drawn previously from biaxial testing carried out by Stella and Sacks in 2007, where the researchers suggested that the ventricularis dominates the mechanical response of the native leaflet in the radial direction at high stress levels (Stella and Sacks, 2007). While the ventricularis is able to withstand high stresses in the radial direction, due to the collagen fibres in the fibrosa having a predominantly circumferential alignment, it is unable to bear as high a load in the radial direction. It is the pairing of the two layers that gives the whole leaflet its stress response in this direction.

Additionally, the ventricularis contains elastin sheets/fibres with some preferential alignment radially. This is necessary for effective leaflet function as the high levels of stretching in the ventricularis in the radial direction allow the valve to close fully under diastolic pressure, while its subsequent elastic recoil ensures a fully open valve during systole (Sacks et al., 2009).

To the authors' knowledge no studies have presented both the mechanical and material response of this tissue, opting either to present a measure of tension or a measure of stress, but the consideration of both of these is needed for effective development of novel materials, especially when considering mimicking both the fibrosa and ventricularis layers. As mentioned, the specialised configuration of the two layers contains folding of the fibrosa and a stretched ventricularis. While this provides the leaflet with an enhanced ability to withstand load and quickly close, the overall stiffness of the leaflet can be described by the individual stiffnesses of the fibrosa and ventricularis layers (see Fig. A4 in supplementary material). When using synthetic materials to replicate the aortic leaflet in future prosthetic devices, it is essential to consider both the mechanical response of the material as well as how the union and combination of these materials may impact the leaflets' behaviour *in vivo*. The need for this structural and mechanical information is evident in publications attempting to mimic both the leaflet fibre microstructure and mechanical response, such as (Coulter et al., 2019; Zeugin et al., 2024; Saidy et al., 2019; Stasiak et al., 2020; Boehm et al., 2023; Snyder and Jana, 2023; Vernon et al., 2022). Lack of a suitable tissue benchmark prevents adequate comparison of novel materials to native tissue. This study addresses this knowledge gap, providing future researchers with the necessary information to drive development of novel materials.

This study does contain a few limitations. The use of uniaxial tensile testing over biaxial tension removed the ability to measure the interaction between fibres in more than one direction. However, the results presented provide a detailed analysis of the mechanical response of the aortic valve leaflet layers and how these drive the response of the whole leaflet. In particular, we have used industrially-relevant methods to show the anisotropy of tissue response between the different orientations and provided quantifiable modulus values for ease of comparison with other materials. Secondly, SHG imaging was limited to the belly and commissure regions of the leaflets. This was due to the knowledge that the collagen fibre bundles originate at the commissures and meet in the belly, providing two high-interest and contrasting regions, as well as the practicality of high imaging and data processing times. Additionally, characterising the fibre structure at the leaflet commissures could provide insight for future prosthetic valve development as the commissure region experiences high levels of stress, a factor known to exacerbate structural valve degeneration (Kostyunin et al., 2020; Stanova et al., 2024). Future work in this area should endeavour to gain the same degree of detailed understanding of the microstructure in the rest of the leaflet. Finally, this entire study was performed on porcine rather than human tissue. While human tissue is preferable, healthy human valve tissue is very difficult to obtain. Porcine tissue is commonly used in valve leaflet research and has been shown to be a good indicator of healthy human valve tissue while also being more readily available (Martin and Sun, 2012).

5. Conclusions

This study has presented an extensive evaluation of the aortic valve leaflet microstructure in combination with mechanical testing to provide further insights into the leaflet material. It has demonstrated, for the first time, the use of clearing agent BABB on aortic valve leaflet tissue to aid SHG imaging, allowing for in-depth quantification of otherwise challenging features of the collagen microstructure. Through this imaging, we have shown that the fibre orientations in the tissue are dependent on leaflet type, while fibre crimp is likely influenced by the local loading environment. Additionally, we have provided detailed quantification of collagen fibre orientations at key regions of the leaflet, as well as collagen fibre crimp in both the fibrosa and ventricularis

layers at these locations. Along with microstructural information, we have provided detailed mechanical property data of the fibrosa and ventricularis layers and how they may individually contribute and influence the loading response of aortic valve leaflets. Overall, this study has provided essential detail to support the current knowledge of the native aortic valve leaflets with the aim to aid the development of next generation bioinspired and biomimicking leaflet designs which can improve upon current commercial devices.

CRediT authorship contribution statement

Celia Hughes: Writing – review & editing, Writing – original draft, Visualization, Validation, Software, Methodology, Investigation, Formal analysis, Conceptualization. **Alix Whelan:** Writing – review & editing, Software, Methodology, Conceptualization. **David O'Reilly:** Writing – review & editing, Supervision, Project administration, Funding acquisition. **Evelyn M. Campbell:** Writing – review & editing, Supervision, Project administration, Funding acquisition. **Caitríona Lally:** Writing – review & editing, Supervision, Resources, Project administration, Funding acquisition, Conceptualization.

Declaration of competing interest

The authors declare the following financial interests/personal relationships which may be considered as potential competing interests: Celia Hughes reports financial support was provided by Boston Scientific Corporation. Alix Whelan reports financial support was provided by Boston Scientific Corporation. David O'Reilly reports financial support was provided by Boston Scientific Corporation. Evelyn Campbell reports financial support was provided by Boston Scientific Corporation. Celia Hughes, Alix Whelan, David O'Reilly, and Evelyn Campbell were employed by Boston Scientific at the time of this work. If there are other authors, they declare that they have no known competing financial interests or personal relationships that could have appeared to influence the work reported in this paper.

Acknowledgements

The authors would like to thank Brenton Kavanaugh (Royal College of Surgeons, Ireland) for his training and expertise on SHG used in this study, and Kenny McNamara (Rosderra Meats, Edenderry) for supplying porcine leaflet tissue. This project is co-funded by the Irish Research Council and Boston Scientific Corporation (EBPPG/2020/200).

Appendix A. Supplementary data

Supplementary data to this article can be found online at https://doi.org/10.1016/j.jmbbm.2024.106881.

Data availability

Data will be made available on request.

References

Balguid, A., Rubbens, M.P., Mol, A., Bank, R.A., Bogers, A.J.J.C., Van Kats, J.P., De Mol, B.A.J.M., Baaijens, F.P.T., Bouten, C.V.C., 2007. The role of collagen cross-links in biomechanical behavior of human aortic heart valve leaflets - relevance for tissue engineering. Tissue Eng. 13, 1501–1511. https://doi.org/10.1089/ten.2006.0279.

Billiar, K.L., Sacks, M.S., 2000. Biaxial mechanical properties of the natural and glutaraldehyde treated aortic valve cusp - Part I: experimental results. J. Biomech. Eng. 122, 23–30. https://doi.org/10.1115/1.429624.

Boehm, C.A., Donay, C., Lubig, A., Ruetten, S., Sesa, M., Fernández-Colino, A., Reese, S., Jockenhoevel, S., 2023. Bio-inspired fiber reinforcement for aortic valves: scaffold production process and characterization. Bioengineering 10, 1064. https://doi.org/10.3390/bioengineering10091064.

Campagnola, P.J., Dong, C.Y., 2011. Second harmonic generation microscopy: principles and applications to disease diagnosis. Laser Photon. Rev. 5, 13–26. https://doi.org/10.1002/lpor.200910024.

Campion, G., Hershberger, K., Whelan, A., Conroy, J., Lally, C., Murphy, B.P., 2021. A biomechanical and microstructural analysis of bovine and porcine pericardium for use in bioprosthetic heart valves. Struct. Hear. 5, 486–496. https://doi.org/10.1080/24748706.2021.1938317.

Chen, X., Nadiarynkh, O., Plotnikov, S., Campagnola, P.J., 2012. Second harmonic generation microscopy for quantitative analysis of collagen fibrillar structure. Nat. Protoc. 7, 654–669. https://doi.org/10.1038/nprot.2012.009.

Coulter, F.B., Schaffner, M., Faber, J.A., Rafsanjani, A., Smith, R., Appa, H., Zilla, P., Bezuidenhout, D., Studart, A.R., 2019. Bioinspired heart valve prosthesis made by silicone additive manufacturing. Matter 1, 266–279. https://doi.org/10.1016/j.matt.2019.05.013.

Gross, L., Kugel, M.A., 1931. Topographic anatomy and histology of the valves in the human heart. Am. J. Pathol. 7, 445–474. PMID: 19969978; PMCID: PMC2062811.

Hepfer, R.G., Chen, P., Brockbank, K.G.M., Jones, A.L., Burnette, A.K., Chen, Z., Greene, E.D., Campbell, L.H., Yao, H., 2018. The impact of heat treatment on porcine heart valve leaflets. Cardiovasc. Eng. Technol. 9, 32–41. https://doi.org/10.1007/s13239-017-0334-x.

Hutson, H.N., Marohl, T., Anderson, M., Eliceiri, K., Campagnola, P., Masters, K.S., 2016. Calcific aortic valve disease is associated with layer-specific alterations in collagen architecture. PLoS One 11, 1–18. https://doi.org/10.1371/journal.pone.0163858.

Iung, B., Delgado, V., Rosenhek, R., Price, S., Prendergast, B., Wendler, O., De Bonis, M., Tribouilloy, C., Evangelista, A., Bogachev-Prokophiev, A., Apor, A., Ince, H., Laroche, C., Popescu, B.A., Piérard, L., Haude, M., Hindricks, G., Ruschitzka, F., Windecker, S., Bax, J.J., Maggioni, A., Hasan-Ali, H., 2019. Contemporary presentation and management of valvular heart disease. Circulation 140, 1156–1169. https://doi.org/10.1161/CIRCULATIONAHA.119.041080.

Johnston, R.D., Gaul, R.T., Lally, C., 2021. An investigation into the critical role of fibre orientation in the ultimate tensile strength and stiffness of human carotid plaque caps. Acta Biomater. 124, 291–300. https://doi.org/10.1016/j.actbio.2021.02.008.

Joyce, E.M., Liao, J., Schoen, F.J., Mayer, J.E., Sacks, M.S., 2009. Functional collagen fiber architecture of the pulmonary heart valve cusp. Ann. Thorac. Surg. 87, 1240–1249. https://doi.org/10.1016/j.athoracsur.2008.12.049.

Kalejs, M., Stradins, P., Lacis, R., Ozolanta, I., Pavars, J., Kasyanov, V., 2009. St Jude Epic heart valve bioprostheses versus native human and porcine aortic valves - comparison of mechanical properties, Interact. Cardiovasc. Thorac. Surg. 8, 553–556. https://doi.org/10.1510/icvts.2008.196220.

Kostyunin, A.E., Yuzhalin, A.E., Rezvova, M.A., Ovcharenko, E.A., V Glushkova, T., Kutikhin, A.G., 2020. Degeneration of bioprosthetic heart valves : update 2020. J. Am. Heart Assoc. 1–19. https://doi.org/10.1161/JAHA.120.018506.

Lazic, S.E., 2010. The problem of pseudoreplication in neuroscientific studies: is it affecting your analysis? BMC Neurosci. 11, 1–17. https://doi.org/10.1186/1471-2202-11-5.

Lee, C.H., Zhang, W., Liao, J., Carruthers, C.A., Sacks, J.I., Sacks, M.S., 2015. On the presence of affine fibril and fiber kinematics in the mitral valve anterior leaflet. Biophys. J. 108, 2074–2087. https://doi.org/10.1016/j.bpj.2015.03.019.

Liao, J., Joyce, E.M., Sacks, M.S., 2008. Effects of decellularization on the mechanical and structural properties of the porcine aortic valve leaflet. Biomaterials 29, 1065–1074. https://doi.org/10.1016/j.biomaterials.2007.11.007.

Manji, R.A., Lee, W., Cooper, D.K.C., 2015. Xenograft bioprosthetic heart valves: past, present and future. Int. J. Surg. 23, 280–284. https://doi.org/10.1016/j.ijsu.2015.07.009.

Martin, C., Sun, W., 2012. Biomechanical characterization of aortic valve tissue in humans and common animal models. J. Biomed. Mater. Res., Part A 100 A, 1591–1599. https://doi.org/10.1002/jbm.a.34099.

Mavrilas, D., Missirlis, Y., 1991. An approach to the optimization of preparation of bioprosthetic heart valves. J. Biomech. 24, 331–339. https://doi.org/10.1016/0021-9290(91)90351-M.

Mega, M., Marom, G., Halevi, R., Hamdan, A., Bluestein, D., Haj-Ali, R., 2016. Imaging analysis of collagen fiber networks in cusps of porcine aortic valves: effect of their local distribution and alignment on valve functionality. Comput. Methods Biomech. Biomed. Eng. 19, 1002–1008. https://doi.org/10.1080/10255842.2015.1088009.

Meijering, E., Jacob, M., Sarria, J.-C.F., Steiner, P., Hirling, H., Unser, M., 2004. Design and validation of a tool for neurite tracing and analysis in fluroescence microscopy images. Cytometry 58A, 167–176. https://doi.org/10.5040/9781474229050.0007.

Misfeld, M., Sievers, H.H., 2007. Heart valve macro- and microstructure. Philos. Trans. R. Soc. B Biol. Sci. 362, 1421–1436. https://doi.org/10.1098/rstb.2007.2125.

Müller-Schweinitzer, E., 2009. Cryopreservation of vascular tissues. Organogenesis 5, 97–104. https://doi.org/10.4161/ORG.5.3.9495.

Otto, C.M., Nishimura, R.A., Bonow, R.O., Carabello, B.A., Rwin, J.P., Gentile, F., Jneid, H., Krieger, ric V., Mack, M., McLeod, C., O'Gara, P.T., Rigolin, V.H., Sundt, T. M., Thompson, A., Toly, C., 2021. ACC/AHA guideline for the management of patients with valvular heart disease: a report of the American College of cardiology/American heart association joint committee on clinical practice guidelines. Circulation 143, E72–E227. https://doi.org/10.1161/CIR.0000000000000923, 2020.

Pei, M., Zou, D., Gao, Y., Zhang, J., Huang, P., 2021. The influence of sample geometry and size on porcine aortic material properties from uniaxial tensile tests using custom-designed tissue cutters , clamps and molds. PLoS One 1–19. https://doi.org/10.1371/journal.pone.0244390.

Pierlot, C.M., Moeller, A.D., Lee, J.M., Wells, S.M., 2015. Biaxial creep resistance and structural remodeling of the aortic and mitral valves in pregnancy. Ann. Biomed. Eng. 43, 1772–1785. https://doi.org/10.1007/s10439-014-1230-2.

Rassoli, A., Fatouraee, N., Zhang, Z., Guidoin, R., 2024. Quantification and comparison of the nonlinear mechanical properties of transcutaneous and human aortic valve leaflets: experimental and numerical studies. Mech. Mater. 188, 104872. https://doi.org/10.1016/j.mechmat.2023.104872.

Rezakhaniha, R., Agianniotis, A., Schrauwen, J.T.C., Griffa, A., Sage, D., Bouten, C.V.C., Van De Vosse, F.N., Unser, M., Stergiopulos, N., 2012. Experimental investigation of collagen waviness and orientation in the arterial adventitia using confocal laser scanning microscopy. Biomech. Model. Mechanobiol. 11, 461–473. https://doi.org/10.1007/s10237-011-0325-z.

Rock, C.A., Han, L., Doehring, T.C., 2014. Complex collagen fiber and membrane morphologies of the whole porcine aortic valve. PLoS One 9, 1–9. https://doi.org/10.1371/journal.pone.0086087.

Sacks, M.S., Smith, D.B., Hiester, E.D., 1998. The aortic valve microstructure: effects of transvalvular pressure. J. Biomed. Mater. Res. 41, 131–141. https://doi.org/10.1002/(SICI)1097-4636(199807)41:1<131::AID-JBM16>3.0.CO;2-Q.

Sacks, M.S., David Merryman, W., Schmidt, D.E., 2009. On the biomechanics of heart valve function. J. Biomech. 42, 1804–1824. https://doi.org/10.1016/j.jbiomech.2009.05.015.

Sadeghinia, M.J., Skallerud, B., Holzapfel, G.A., Prot, V., 2022. Biomechanics of mitral valve leaflets: second harmonic generation microscopy, biaxial mechanical tests and tissue modeling. Acta Biomater. 141, 244–254. https://doi.org/10.1016/j.actbio.2022.01.003.

Saidy, N.T., Wolf, F., Bas, O., Keijdener, H., Hutmacher, D.W., Mela, P., De-Juan-Pardo, E.M., 2019. Biologically inspired scaffolds for heart valve tissue engineering via melt electrowriting. Small 15, 1–15. https://doi.org/10.1002/smll.201900873.

Schindelin, J., Arganda-Carreras, I., Frise, E., Kaynig, V., Longair, M., Pietzsch, T., Preibisch, S., Rueden, C., Saalfeld, S., Schmid, B., Tinevez, J.Y., White, D.J., Hartenstein, V., Eliceiri, K., Tomancak, P., Cardona, A., 2012. Fiji: an open-source platform for biological-image analysis. Nat. Methods 9, 676–682. https://doi.org/10.1038/nmeth.2019.

Schriefl, A.J., Wollinski, H., Regitnig, P., Kohlwein, S.D., Holzapfel, G.A., 2013. An automated approach for three-dimensional quantification of fibrillar structures in optically cleared soft biological tissues. J. R. Soc. Interface 10. https://doi.org/10.1098/rsif.2012.0760.

Snyder, Y., Jana, S., 2023. Electrospun elastomeric leaflet substrates that structurally and mechanically mimic human aortic valve leaflets. ACS Appl. Polym. Mater. 5, 3749–3761. https://doi.org/10.1021/acsapm.3c00385.

Stanova, V., Rieu, R., Thollon, L., Salaun, E., Rodes-Cabau, J., Cote, N., Mantovani, D., Pibarot, P., 2024. Leaflet mechanical stress in different designs and generations of transcatheter aortic valves: an in vitro study. Struct. Hear. 8. https://doi.org/10.1016/j.shj.2023.100262.

Stasiak, J.R., Serrani, M., Biral, E., Taylor, J.V., Zaman, A.G., Jones, S., Ness, T., De Gaetano, F., Costantino, M.L., Bruno, V.D., Suleiman, S., Ascione, R., Moggridge, G. D., 2020. Design, development, testing at ISO standards and: in vivo feasibility study of a novel polymeric heart valve prosthesis. Biomater. Sci. 8, 4467–4480. https://doi.org/10.1039/d0bm00412j.

Stella, J.A., Sacks, M.S., 2007. On the biaxial mechanical properties of the layers of the aortic valve leaflet. J. Biomech. Eng. 129, 757–766. https://doi.org/10.1115/1.2768111.

Stradins, P., Lacis, R., Ozolanta, I., Purina, B., Ose, V., Feldmane, L., Kasyanov, V., 2004. Comparison of biomechanical and structural properties between human aortic and pulmonary valve. Eur. J. Cardio. Thorac. Surg. 26, 634–639. https://doi.org/10.1016/j.ejcts.2004.05.043.

Tornifoglio, B., Johnston, R.D., Stone, A.J., Kerskens, C., Lally, C., 2023. Microstructural and mechanical insight into atherosclerotic plaques: an ex vivo DTI study to better assess plaque vulnerability. Biomech. Model. Mechanobiol. 22, 1515–1530. https://doi.org/10.1007/s10237-022-01671-5.

Torun, S.G., Munoz, P. de M., Crielaard, H., Verhagen, H.J.M., Kremers, G.J., van der Steen, A.F.W., Akyildiz, A.C., 2023. Local characterization of collagen architecture and mechanical failure properties of fibrous plaque tissue of atherosclerotic human carotid arteries. Acta Biomater. 164, 293–302. https://doi.org/10.1016/j.actbio.2023.04.022.

Ueda, H.R., Dodt, H.-U., Osten, P., Economo, M.N., Chandrashekar, J., Keller, P.J., 2020. Whole-brain profiling of cells and circuits in mammals by tissue clearing and light-sheet microscopy. Neuron 106, 369–387. https://doi.org/10.1016/j.neuron.2020.03.004.

Vernon, M.J., Lu, J., Padman, B., Lamb, C., Kent, R., Mela, P., Doyle, B., Ihdayhid, A.R., Jansen, S., Dilley, R.J., De-Juan-Pardo, E.M., 2022. Engineering heart valve interfaces using melt electrowriting: biomimetic design strategies from multi-modal imaging. Adv. Healthcare Mater. 11, 1–17. https://doi.org/10.1002/adhm.202201028.

Vesely, I., 1997. The role of elastin in aortic valve mechanics. J. Biomech. 31, 115–123. https://doi.org/10.1016/S0021-9290(97)00122-X.

Vesely, I., Noseworthy, R., 1992. Micromechanics of the fibrosa and the ventricularis in aortic valve leaflets. J. Biomech. 25, 101–113. https://doi.org/10.1016/0021-9290(92)90249-Z.

Whelan, A., 2021. Investigation into the collagen fibre-mediated fatigue mechanics of bovine pericardium for use in bioprosthetic heart valves. PhD Thesis. Trinity College Dublin. http://www.tara.tcd.ie/xmlui/handle/2262/95806.

Whelan, A., Duffy, J., Gaul, R.T., O'Reilly, D., Nolan, D.R., Gunning, P., Lally, C., Murphy, B.P., 2019. Collagen fibre orientation and dispersion govern ultimate tensile strength, stiffness and the fatigue performance of bovine pericardium. J. Mech. Behav. Biomed. Mater. 90, 54–60. https://doi.org/10.1016/j.jmbbm.2018.09.038.

Whelan, A., Williams, E., Nolan, D., Murphy, B., Gunning, P., O'Reilly, D., Lally, C., 2021. Bovine pericardium of high fibre dispersion has high fatigue life and increased collagen content; potentially an untapped source of heart valve leaflet tissue. Ann. Biomed. Eng. 49, 1022–1032. https://doi.org/10.1007/s10439-020-02644-4.

Zeugin, T., Coulter, F.B., Gülan, U., Studart, A.R., Holzner, M., 2024. In vitro investigation of the blood flow downstream of a 3D-printed aortic valve. Sci. Rep. 14, 1–12. https://doi.org/10.1038/s41598-024-51676-6.